Herrn Prof. Dr. R. WIENECKE danke ich für seine Förderung und das Interesse, das er dieser Arbeit entgegenbrachte. Herrn Dr. D. PFIRSCH und Herrn Dr. H. TASSO bin ich für wertvolle Ratschläge und Diskussionen dankbar. Ebenso danke ich Herrn H. GORENFLO für die Durchführung der numerischen Rechnungen. — Diese Arbeit wurde im Rahmen des Vertrages zwischen dem Institut für Plasmaphysik und der Europäischen Atomgemeinschaft über die Zusammenarbeit auf dem Gebiete der Plasmaphysik durchgeführt.

Hydrogen Plasma Production by Giant Pulse Lasers *

PETER MULSER

Institut für Plasmaphysik, Garching bei München

(Z. Naturforsch. **25 a**, 282—295 [1970]; received 5 December 1969)

The problem of interaction of an intense laser beam with solid hydrogen is theoretically investigated in a one-dimensional plane geometry. The time dependent distributions of density, temperature and velocity of the produced plasma as well as those of the solid are found by numerical solution of the hydrodynamic equations for various laser powers. The maximum temperature can be approximately expressed in closed form as a function of the laser intensity and time. The calculations allow for the influence of thermal conduction and viscosity. At laser intensities above 1.8×10^{11} W/cm² the plasma frequency rises above that of the laser in the transition sheath between the hot plasma and the cold solid. The problem of absorption and reflection of laser radiation in this region is investigated.

I. Introduction

Nowadays giant pulse lasers reach intensities of 10^{12} W/cm² and more if focused with lenses of suitable focal length to an area of 10^{-4} cm². Emission thereby lasts between about 2 and 50 nsec. The interaction of such radiation fields with matter greatly differs from the usual picture of low-intensity electromagnetic waves passing through a medium. Numerous experiments since 1963 have demonstrated that a sufficiently intense laser will make transparent dielectrics opaque and cause a hot, dense plasma cloud to form on the surface.

Near the ruby laser frequency ($\omega = 2.73\times10^{15}$ sec^{-1}) many insulators such as hydrogen appear completely transparent; with normal light sources their coefficients of absorption are almost zero. If, however, there are some free electrons in the insulator, these in the intense radiation field of a laser can gain so much energy that they quickly increase in number as a result of collisional ionization, and strong absorption occurs. CARUSO et al. [1], for example, have calculated that at a radiation intensity of 10^{11} W/cm² a 100 μ thick hydrogen foil becomes opaque in less than 10^{-10} sec if there are 10^6 free electrons per cm³ present when irradiation begins, i. e. a vanishingly small number compared with the number of atoms, which for solid hydrogen is 4.5×10^{22} cm^{-3}. No matter where the first free electrons originate — whether from multiphoton absorption, from impurities in which they were loosely bound or from external charging — it was found experimentally time and again that with sufficient laser intensity a highly absorbent layer of free electrons forms in a very short time. Any study of subsequent processes will therefore start from a certain initial ionization.

In the field of fusion research one is mainly interested in the complete evaporation of solid or liquid drops of low atomic weight in a focused laser beam. The production, heating, and expansion of such a plasma was therefore studied theoretically in a spherical model on the assumption that the matter in the focus is fully ionized from the outset, and that the energy input is uniformly absorbed in the drop as long as its diameter does not exceed that of the focus as a result of expansion [2–4].

* Auszug aus der von der Fakultät für Maschinenwesen und Elektrotechnik der Technischen Hochschule München zur Erlangung des akademischen Grades eines Doktors der Naturwissenschaften genehmigten Dissertation über „Erzeugung von Wasserstoffplasma durch Riesenimpulslaser" des Dipl.-Phys. PETER MULSER. Tag der Promotion 31. 7. 1969.

Sonderdruckanforderungen an Dr. P. MULSER, Institut für Plasmaphysik, Experimentelle Plasmaphysik 3, *D-8046 Garching* bei München.

[1] A. CARUSO, B. BERTOTTI, and P. GIUPPONI, Nuovo Cim. **45** B, 176 [1966].
[2] J. M. DAWSON, Phys. Fluids **7**, 981 [1964].
[3] A. F. HAUGHT and D. H. POLK, Phys. Fluids **9**, 2047 [1966].
[4] W. J. FADER, Phys. Fluids **11**, 2200 [1968].

The assumption of uniform energy absorption greatly facilitates calculation of heating and expansion and affords useful information on the properties of the plasma after a lengthy period of time. It does not, however, provide a satisfactory answer to the physically interesting question in what way and how quickly the solid is converted to plasma at high laser intensities. A major advance in this direction was made by AFANASYEV et al[5], who investigated plasma production in plane geometry, and then by CARUSO et al.[6]. These authors consider the case of a time constant light flux incident on the surface of a solid occupying a half-space and then make a dimensional analysis of the dynamic process. This allows the plasma parameters averaged in space to be determined in closed form as functions of the laser intensity, time, and absorption coefficient.

In order, however, to determine the distributions of the density, temperature, and velocity of the plasma produced, the local conservation laws of hydrodynamics have to be solved simultaneously with the equations of optics. Only thus is it possible to treat such questions as the influence of thermal conduction and viscosity, propagation and reflection of light in the high density region, recombination in the plasma, or the problem of ponderomotive forces[7].

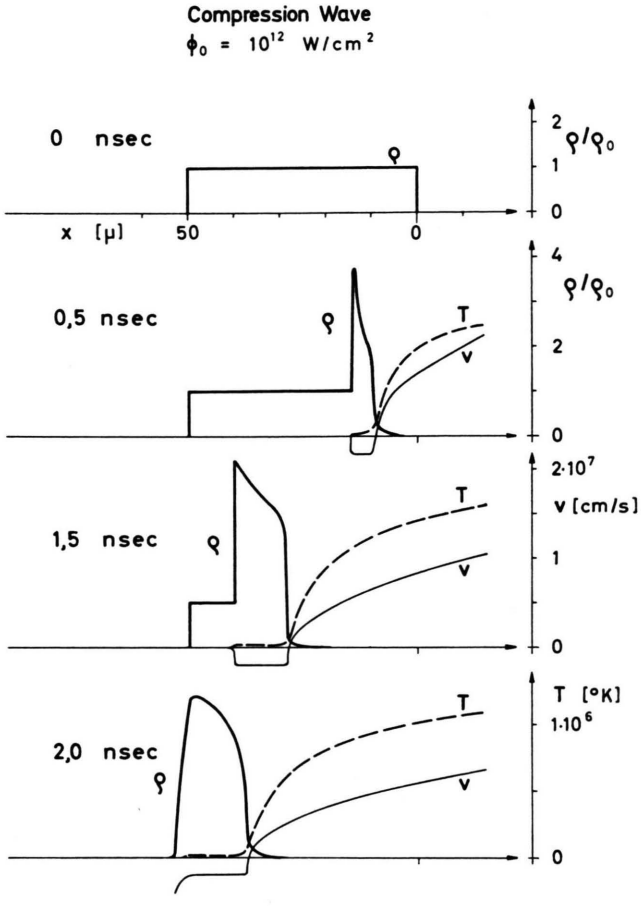

Fig. 1. Shock wave in solid hydrogen at various times for $\Phi_0 = 10^{12}$ W/cm². The shock velocity is 2.7×10^6 cm/sec. Undistrubed foil above. Irradiated from the right.

II. The Model

Basic physical information is ensured by making all calculations one-dimensional and using laser pulses of constant intensity. For this purpose we consider an infinitely extended foil of thickness D and initial density ϱ_0 on the one surface of which a laser of constant power density Φ_0 is incident starting at the time $t=0$ (Fig. 1). A small number of free electrons should be present in the foil so that a noticeable fraction of the light can be absorbed from the outset and is converted into heat. This causes a change in the number of free electrons and hence in the light absorption; in addition a strong pressure gradient forms at the surface and matter escapes into the vacuum. Part of the laser light can now penetrate more deeply into the target, to the extent to which the expanding plasma becomes rarefied, and heats more matter.

This gasdynamic process can be adequately described in a one-fluid model taking thermal conductivity and viscosity into account. For this purpose all parameters of interest such as the density ϱ, velocity v, pressure p, energy per unit mass ε, and laser intensity Φ are expressed as functions of the Lagrange parameter a and the time t, where a is chosen such that x is identical with a at the time $t=0$, i. e. a is the initial position of the volume element under consideration. The laws of conservation of mass, monentum, and energy (see, for example[8], Vol. I, p. 4 et seq. and p. 71)

[5] YU. V. AFANASYEV, O. N. KROKHIN, and G. V. SKLIZKOV, IEEE J. Quant. El. QE−**2**, 483 [1966].
[6] A. CARUSO and R. GRATTON, Plasma Phys. **10**, 867 [1968].
[7] H. HORA, Phys. Fluids **12**, 182 [1969].
[8] YA. B. ZELDOVICH and YU. P. RAIZER, Physics of Shock Waves and High-Temperature Hydrodynamic Phenomena, Acad. Press, New York 1966.

$$\varrho_0 = \varrho(\partial x/\partial a), \tag{1}$$

$$\varrho_0 \frac{\partial v}{\partial t} = \frac{\partial}{\partial a}\left\{-p + \frac{4}{3}\frac{\varrho}{\varrho_0}\mu\frac{\partial v}{\partial a}\right\}, \tag{2}$$

$$\varrho_0 \frac{\partial \varepsilon}{\partial t} = \frac{\partial \Phi}{\partial a} + \frac{\partial}{\partial a}\left(\frac{\varrho}{\varrho_0}\varkappa\frac{\partial T}{\partial a}\right) + \left\{-p + \frac{4}{3}\frac{\varrho}{\varrho_0}\mu\frac{\partial v}{\partial a}\right\}\frac{\partial v}{\partial a} \tag{3}$$

together with the relation for the velocity

$$v(a,t) = \partial x(a,t)/\partial t \tag{4}$$

then afford a complete description of the processes involved. The coefficients of viscosity and thermal conductivity are denoted by μ and $\varkappa$ in Eqs. (2) and (3). The three terms at the r.h.s. of energy equation represent consecutively energy input due to irradiation, thermal conduction, and mechanical work. In the energy range under consideration the radiation losses of the plasma are small and are not taken into account, cf. [2].

All of the calculations here apply to hydrogen. The number of free electrons is expressed in terms of the degree of ionization, which is defined as the ratio $\eta = n_e/(n_n + n_i) = n_e/n_H$, where n_n is the neutral particle density and n_H the total number of hydrogen nuclei per unit volume. Quasi-neutrality is thereby assumed, i. e. $n_e \approx n_i$. n_H, T and η are related by the Sahy equation (see Section V):

$$\frac{\eta}{1-\eta} = \left(\frac{2\pi m_e k}{h^2}\right)^{3/2} \frac{T^{3/2}\exp\{-U_i/kT\}}{n_H}. \tag{5}$$

Here the partition-function ratio for ions and hydrogen atoms $\Sigma^+/\Sigma^0 = 1/2$ was used. As an equation of state we take the ideal gas law for the plasma as well as for the high density region:

$$p = (1+\eta) n_H k T. \tag{6}$$

The internal energy per unit mass is then the sum of the thermal energy and ionization energy:

$$\varepsilon = \frac{1}{m_H}\left\{\frac{3}{2}(1+\eta)kT + U_i\eta\right\} \tag{7}$$

(m_H = mass of hydrogen atom, U_i = ionization energy per atom). In order to satisfy the energy balance, the ionization energy of the atomic hydrogen is increased by half the dissociation energy of H_2, i. e. $U_i = 13.6 + 2.24 = 15.84$ eV. The local light intensity $\Phi(x,t)$ should be related to the laser intensity Φ_0 by the absorption law

$$\Phi(x,t) = \Phi_0 \exp\left\{-\int_x^\infty \alpha(x,t)\,dx\right\}; \tag{8}$$

$\alpha(x,t)$ denotes the local absorption coefficient. (For α and the validity of Eq. (8) see Appendix I and Section IV.) According to [9], p. 462, the viscosity μ is given by the following expression:

$$\mu \approx \mu_i = 1.365\frac{3 m_i^{1/2} k^{5/2}}{4(2\pi)^{1/2} e^4}\frac{T^{5/2}}{\ln\Lambda}\ [\text{cgs grad}]\ .$$

The coefficient of thermal conductivity according to [10] is

$$\varkappa = 20\left(\frac{2}{\pi}\right)^{3/2}\frac{k^{7/2}\varepsilon\delta_T}{m_e^{1/2}e^4}\frac{T^{5/2}}{\ln\Lambda} \qquad [\text{cgs grad}]$$

with $\varepsilon = 0.4189$ and $\delta_T = 0.2252$. $\ln\Lambda$ is calculated in all transport parameters according to the following formulae [11]:

$$\Lambda = \Lambda_K = \frac{3 k^{3/2} T^{3/2}}{2 e^3 \pi^{1/2} n_e^{1/2}} \quad \text{for } T \leqq 4.2\times 10^5\ ^\circ\text{K},$$

$$\Lambda = \left(\frac{4.2\times 10^5}{T}\right)^{1/2}\Lambda_K \quad \text{for } T \geqq 4.2\times 10^5\ ^\circ\text{K}.$$

All calculations are made for ruby laser step pulses, i. e. the laser starts with the intensity Φ_0 at the time $t = 0$, and this remains constant for the entire heating period. The density of solid hydrogen ϱ_0 is chosen as initial density, and for $t = 0$ the temperature T and flow velocity v are everywhere set equal to zero; the thickness of the foil is assumed to be $D = 50\,\mu$. An initial degree of ionization $\eta = 7\times 10^{-3}$ was chosen. The numerical calculations were performed for intensities $\Phi_0 = 10^{11}$, 10^{12} and 10^{13} W/cm^2. The numerical integration method is outlined in Appendix II.

III. Numerical Results

The shock wave: As soon as the foil is exposed to laser radiation some of the light is absorbed and converted into internal energy, η increasing in accordance with the Saha equation (5). As a result, 50 μ foils quickly become opaque at laser intensities $\Phi_0 = 10^{11}$ W/cm^2, because with the rising number of free electrons the absorbing region reduces to a small layer at the surface and hot plasma streams off into space. At a power density $\Phi_0 = 10^{12}$ W/cm^2

[9] I. P. SHKAROFSKY, T. W. JONSTON, and M. P. BACHYNSKI, The Particle Kinetics, Addison-Wesley Publ. Co., Reading Mass. 1966.

[10] L. SPITZER and R. HÄRM, Phys. Rev. **89**, 977 [1953].

[11] L. SPITZER, Physics of Fully Ionized Gases, Intersc. Publishers, Inc., New York 1956.

a pressure of over 300 kbar builds up in less than 0.2 nsec in the region of strongest light absorption, and a shock wave with a velocity of 2.7×10^6 cm/sec is formed in the foil (Fig. 1; the laser is directed from the right). Behind the shock front the hydrogen, now compressed in a ratio of about 1 : 4, has attained the temperature 1.5×10^4 °K. After 2 nsec the compression wave reaches the free back surface of the 50 μ foil, a rarefraction wave runs back to the right, and the foil as a whole begins to move. The shock velocity depends, of course, on the laser power. At $\Phi_0 = 10^{11}$ W/cm^2 it is 1.1×10^6 cm/sec and at $\Phi_0 = 10^{13}$ W/cm it is 6.7×10^6 cm/sec. The compression ratio in all cases is about 4, as it should be for strong shocks in atomic gases ($\gamma = c_p/c_v = 5/3$). The shock wave in Fig. 1 has a somewhat different profile to that in [12] because the Saha equation was used here with the result that γ is no longer constant everywhere.

The hot plasma: On the laser side of the compressed foil the density drops sharply as a result of the strong temperature rise caused by heating. Fig. 2 shows the spatial distribution of plasma density, temperature, laser intensity, and velocity for $\Phi_0 = 10^{12}$ W/cm^2 at the times 2, 7, 12, 20, and 30 nsec. The left ends of these curves have to be imagined as joining on to the points in Fig. 1 where the density (normalized to the undisturbed solid) has the value 1. Because of the high electron density this is also the region of strongest absorption, as can be seen from the diagram for the laser intensity. All curves show similar behaviour here: The transition region is characterized by very high gradient of density, temperature and velocity which only decrease slightly at later times. As seen above the total conservation of momentum causes the foil to recede to the left. This is indicated in Fig. 2 by the pronounced displacement of the curves relative to one another. For the same reason more and more plasma streams to the left with time (negative velocities in the fourth diagram of Fig. 2). After about 55 nsec the foil is completely evaporated and transformed into plasma. Very similar diagrams are obtained for other power densities. Fig. 3 gives the temperature distribution at various times for $\Phi_0 = 10^{13}$ W/cm^2. The time development of the temperature maximum for three different power levels can be seen in Fig. 4 (solid curves).

The quantity of plasma produced is shown in Fig. 5 as a function of time. The right ordinate gives the number N of atoms evaporated from an area of 10^{-4} cm^2. On the left ordinate the corresponding depth d of the evaporated layer is plotted. The foil is completely converted into plasma as soon as d reaches the value 50 μ. The increase of d per unit time is equivalent to a velocity much smaller than that of the shock wave. This velocity after 10 nsec, for example, is $\dot{d} = 1.04 \times 10^5$ cm/sec for $\Phi_0 = 10^{12}$ W/cm^2.

As a result of the large difference in density between plasma and compressed solid (see Fig. 1 and 2) it follows that the major part of the incident laser energy is transferred to the plasma. In fact only about 8% of energy go into the dense cold phase. During irradiation and as long as there is still a residue of cold matter present the ratio of the total thermal and kinetic energy is about 45% to 55%.

Similarity relations: In [5, 6] a dimensional analysis is made for the parameters of interest when heating infinitely thick foils. This is successful on the assumption that the heating process does not depend on the following parameters: initial density, ionization energy, thermal conductivity and viscosity. The following relation is then obtained for the quantity of plasma produced:

$$N \sim \Phi_0^{1/2} t^{3/4}. \tag{9}$$

Although all the above mentioned parameters are allowed for in our computations it can be seen from Fig. 5 that the relation (9) is very well satisfied. The two bottom curves deviate so little that they could not be plotted separately. For $\Phi_0 = 10^{13}$ W/cm^2 the dependence can no longer be described exactly by (9), but the deviations can largely be ascribed to the finite foil thickness. The proportionality constant can only be obtained by numerical calculation, and it deviates from that determined in [5, 6] (in [5] a factor of about 2; cf. [13], Fig. 2). If it is assumed that the sets of curves in Fig. 2 are similar to one another at other time independent laser intensities, a relation for the maximum temperature $T_{\max}$ can be derived:

$$T_{\max} \sim \Phi_0^{1/2} t^{1/4}. \tag{10}$$

This relation is also well satisfied (Fig. 4). If we apply a laser intensity of $\Phi_0 = 10^{12}$ W/cm^2 and

[12] P. MULSER and S. WITKOWSKI, Phys. Letters **28** A, 703 [1969].

[13] P. MULSER and S. WITKOWSKI, Phys. Letters **28** A, 151 [1968].

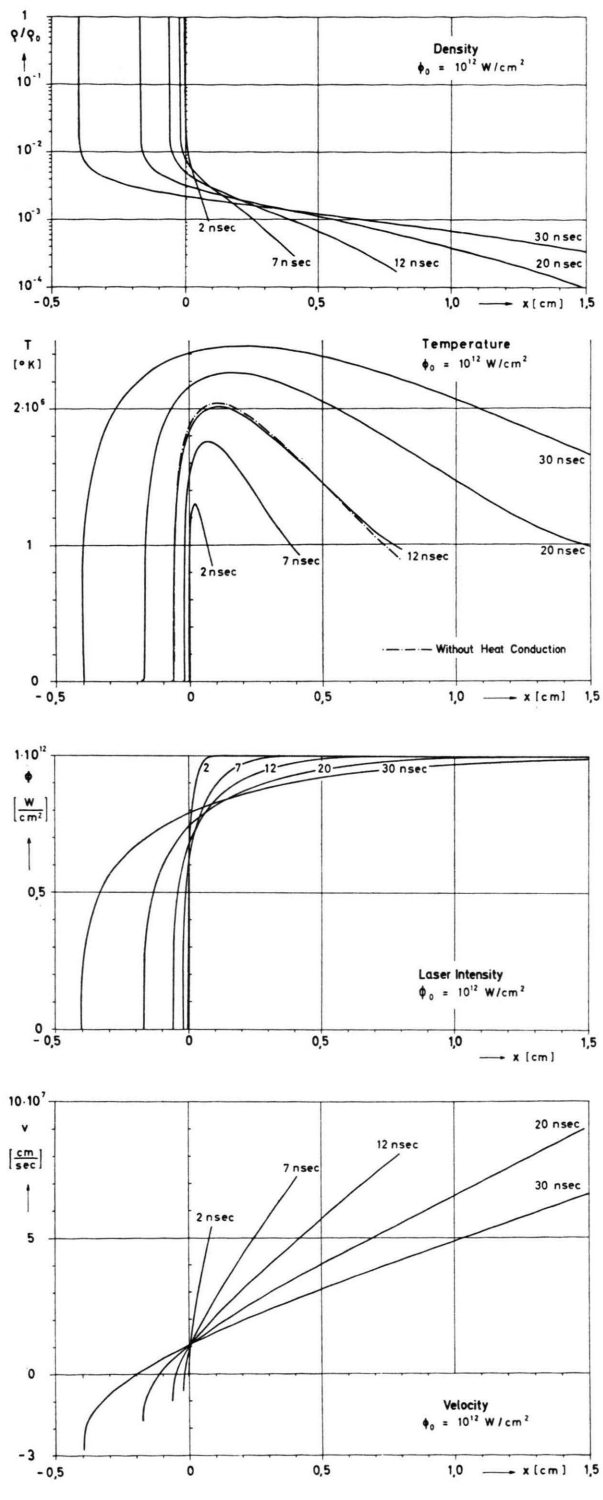

Fig. 2. Plasma density (normalized to solid; log scale), temperature, laser intensity, and velocity distributions at various times. Irradiated from the right. $\Phi_0 = 10^{12}$ W/cm².

choose the proportionality constant so that $T_{\max}$ from Eq. (10) coincides at 15 nsec with the value determined numerically without thermal conduction, these curves lie between the solid and dash-and-dot curves. At $\Phi_0 = 10^{11}$ W/cm² the influence of the ionization energy causes a small deviation: The true temperature (solid curve) lies below the curve calculated from the relation (10), where the ionization energy is disregarded. The largest deviations from (10) again occur at $\Phi_0 = 10^{13}$ W/cm² due to the finite thickness of the target.

Influence of thermal conductivity and viscosity: The numerical calculations with and without viscosity show deviations of a maximum of 4% only at $\Phi_0 = 10^{13}$ W/cm². The mean deviation is less than 1%. More important is the influence of thermal conductivity. For comparison the numerical results without thermal conduction are plotted (dash-and-dot curves) in Figs. 2, 3, 4, and 5: its influence is best pronounced at the highest intensity $\Phi_0 = 10^{13}$ W/cm² but does not exceed a few percent. At lower intensities it is still smaller and can be neglected.

IV. On the Reflection of the Laser Light

The use of the absorption coefficient in Appendix I in conjunction with the Saha equation leads to the high spatial gradients in the transition region (Fig. 2), where the normalized density increases from 2×10^{-2} to 1. The transition from given to complete ionization in the intensity range considered occurs between 0.6 and 1 μ, i. e. over about a vacuum wavelenght of the ruby laser. This causes appreciable changes of the refractive index (4a) (Appendix I) over a wavelenght. In addition, the plasma frequency ω_p exceeds the light frequency up to a factor of 3 in this region. The question arises how the light propagates in the transition region. Appreciable reflection is sure to be encountered here. As far as the author is aware, the problem has only been treated once before in this connection, by assuming the simplifying WKB condition [14]. For layers of such high optical inhomogeneity the wave structure of the light has to be allowed for in calculating reflection and absorption. This means in our case that in the transition region the wave Eq. (2a) would have to be solved simultaneously with the equations of motion (1), (2),

[14] J. DAWSON, P. KAW, and B. GREEN, Phys. Fluids **12**, 875 [1969].

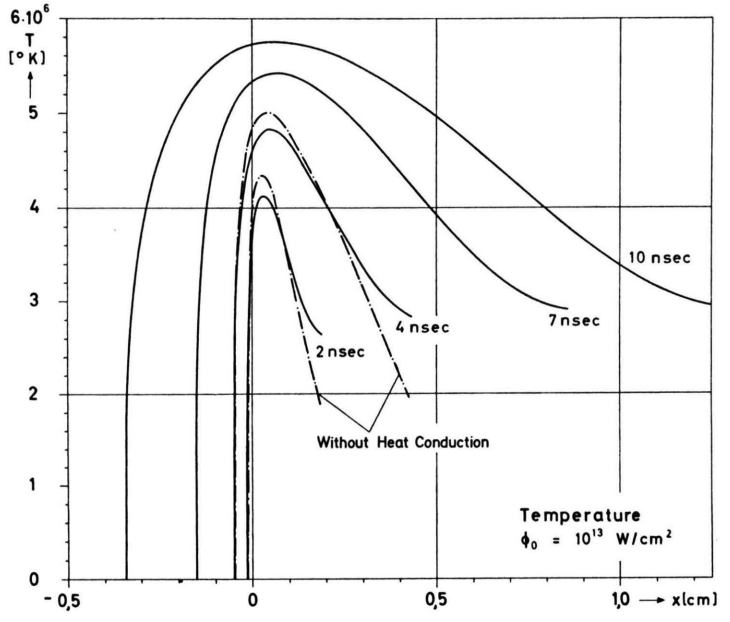

Fig. 3.

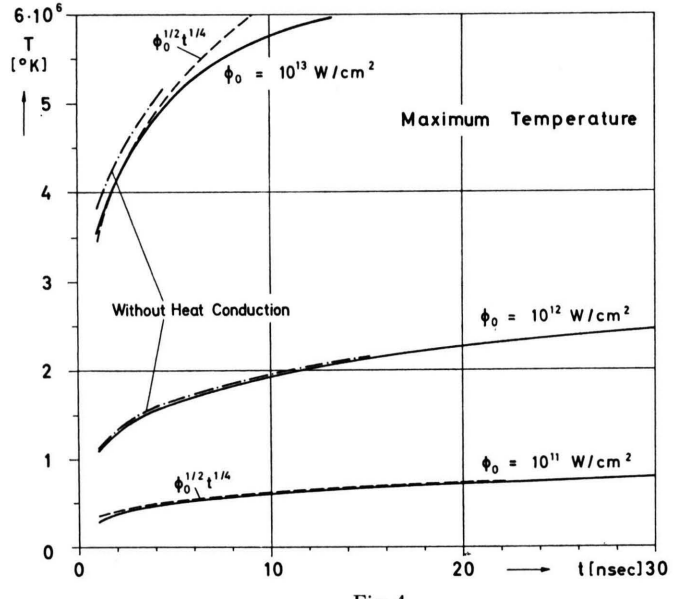

Fig. 4.

Fig. 3. 50 μ foil. Temperature distribution for power density $\Phi_0 = 10^{13}$ W/cm².

Fig. 4. Time development of the temperature maximum for $\Phi_0 = 10^{11}$, 10^{12}, and 10^{13} W/cm². $T_{max} \sim \Phi_0^{1/2} t^{1/4}$.

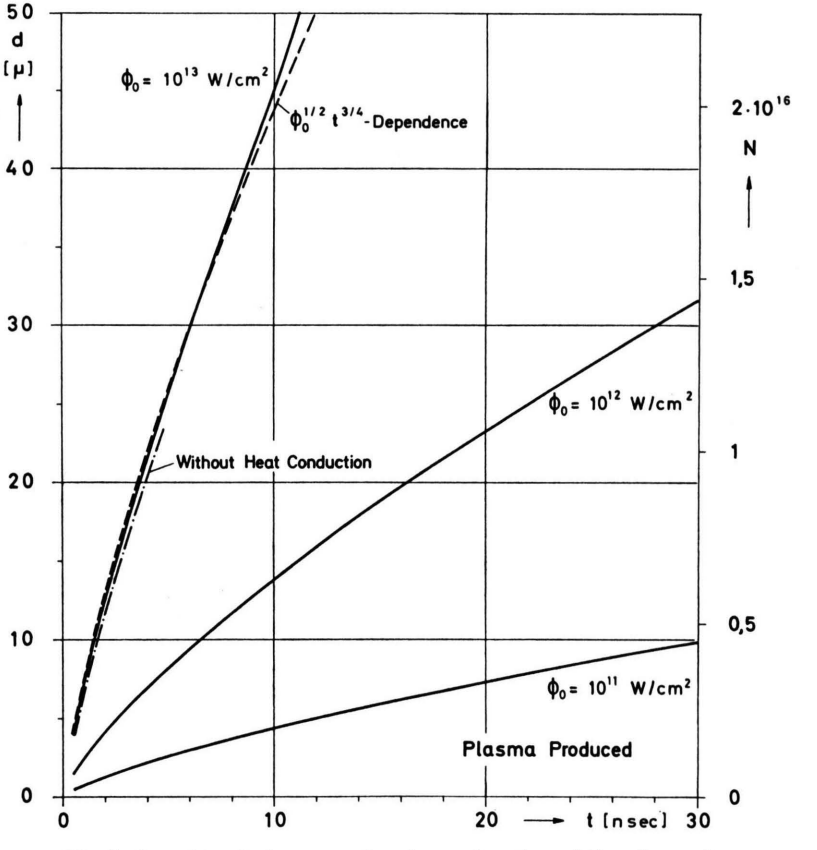

Fig. 5. Quantity of plasma produced as a function of time for various intensities. Left ordinate: thickness of evaporated layer; right ordinate: particle number per 10^{-4} cm². Relation $N \sim \Phi_0^{1/2} t^{3/4}$ is very well satisfied.

and (3). Since this is a cumbersome procedure, only time independent density profiles (fitted to the numerical results described above) for purely transverse electromagnetic waves are investigated in the following. In the numerical results of Section III the elctron density rises steeply to a maximum in the region of greatest absorption and then drops very quickly to almost zero towards the shock wave. The real part of the refractive index varies as follows: In the low density plasma $\mathrm{Re}(n^2)$ is only slightly below 1; with increasing electron density it tends to zero or may even drop below it; finally, in the shocked region it resumes a value of about 1 (the value in solid hydrogen is $n = 1.112$). We therefore consider an inhomogeneous layer of thickness d in which the particle density is determined by

$$n_{\mathrm{H}} = n_{\mathrm{H}}^{0} \sin^2\left(\frac{\pi x}{2d}\right) \qquad -d \leqq x \leqq 0$$

and the temperature by

$$T = T_0 \cos^2\left(\frac{\pi x}{2d}\right) \qquad -d \leqq x \leqq 0\,.$$

The number of free electrons is again governed by the Saha Eq. (5). The value $5 \times 10^5\ ^{\circ}\mathrm{K}$ was chosen for T_0, while n should cover the range from 10^{21} to a few $10^{22}\,\mathrm{cm}^{-3}$. The local refractive index n is then determined by (4a) of Appendix I. On the left and right of the profile n should be $n = 1$.

The Maxwell equations yield the energy conservation law in the following way:

$$\mathfrak{j}\,\mathfrak{E} + \varepsilon_0 c^2 \nabla\,(\mathfrak{E} \times \mathfrak{B}) + \frac{\partial}{\partial t}\left\{\tfrac{1}{2}\,\varepsilon_0\,\mathfrak{E}^2 + \tfrac{1}{2}\,\varepsilon_0 c^2 \mathfrak{B}^2\right\} = 0\,.$$

In real notation $\mathfrak{j}\,\mathfrak{E}$ thereby represents the work irreversibly performed by the electromagnetic field per unit time and volume. Since we set $E = E(x)e^{-i\omega t}$ and, accordingly, $\mathfrak{j}$ complex, this yields for the light absorption averaged over an oscillation period

$$\frac{\partial \Phi}{\partial x} = \langle \mathrm{Re}(j) \cdot \mathrm{Re}(E) \rangle = \tfrac{1}{2}\,\mathrm{Re}(\sigma)\,E\,E^{*}. \qquad (11)$$

E has to satisfy the stationary wave Eq. (2a), and σ is related to n by (3a). The simple absorption law $\partial\Phi/\partial x = \alpha\,\Phi$ following from Eq. (8) and taken as basis for the numerical calculation in Section III thus has to be replaced in strongly inhomogeneous media by the relation (11). In the case of weak optical inhomogeneity, of course, relation (11) leads back to the expression (8). In order to solve the wave equation, which can only be done numerically for the above profiles, one has to satisfy the condition that only a transmitted wave may occur behind the layer. The wave equation is therefore split into the equivalent first-order system:

$$(E^- + E^+)' = i\,k(E^- - E^+),$$
$$(E^- - E^+)' = i\,k\,n^2(E^- + E^+).$$

Where $E^+ + E^- = E$ (see [15], p. 11). Here, in front of the layer ($x \geqq 0$), E^- denotes the laser wave and $E^+(x)$ the wave reflected by the layer. On the side of the emerging wave ($x = -d$) we have to set $E^+ = 0$. The reflection and transmission coefficients R and Tr are calculated from

$$R = \left(\frac{E^+ E^{+*}}{E^- E^{-*}}\right)_{x=0} \quad \text{and} \quad Tr = \frac{(E^- E^{-*})_{x=-d}}{(E^- E^{-*})_{x=0}}\,.$$

The results for four profiles with different values of n_{H}° are shown in Fig. 6. The bottom curve in each case gives the variation of the real part of n^2 in a layer of thickness $d = \lambda$. As long as the electron density n_{e} remains everywhere below the value $2.34 \times 10^{21}\,\mathrm{cm}^{-3}$, the plasma frequency is lower than the ruby laser frequency ω, and $\mathrm{Re}(n^2)$ is positive everywhere. This is the case in the top two pictures; in the bottom two pictures the electron density reaches higher values inside the layer, and $\mathrm{Re}(n^2)$ becomes negative. At the boundaries $x = 0$ and $x = -d$ of the layer the electron density drops to zero and n^2 continuously attains the value 1. The curve denoted by $|E|$ gives the magnitude of the electric field $|E^- + E^+|$ for a monochromatic wave with amplitude $|E^-| = 5$ units that is incident from the right (dashed line in Fig. 6). The total coefficients of reflection R, transmission Tr, and absorption A of the profiles are given at the bottom of each picture. R remains below 25% as long as the plasma frequency is everywhere below the light frequency. In the four layers drawn there is superposition of the incident and reflected waves so that $|E|$ appears to be modulated and elevated in part, in the fourth picture by a factor of almost 2. The curve denoted by $A(x)$ represents for every point the energy absorbed in the layer up to this point; $\langle \mathrm{Re}(j) \cdot \mathrm{Re}(R) \rangle$ determines the slope of $A(x)$. Calculating the absorbed energy for the profiles in question according to the WKB approximation (8) still yields good agreement with Eq. (11) for the

[15] P. MULSER, IPP 3/85 [1969].

first picture, but the deviations grow with increasing reflection. Equation (8) would give the strongest absoprtion for the profile with the highest electron density, which is not at all the case using the exact Eq. (11): Because of the strong reflection in the latter case only a little light penetrates into the region of high electron density, and there is a decrease in absorption.

The transmission Tr, reflection R, and absorbed energy A for such inhomogeneous layers of thickness $d = 0.5\,\lambda$, $1\,\lambda$, $1.5\,\lambda$, and $2\,\lambda$ are shown in Fig. 7. The curves result from the fact that for each profile thickness n_H° covers the whole range from 10^{21} to a few $10^{22}\,\mathrm{cm}^{-3}$. In each case we chose as abscissa the square of the maximum normalized plasma frequency $(\omega_p/\omega)^2$ since, with constant T_0 of course, $(\omega_p/\omega)^2$ is a function of n only. With increasing electron density the transmission quickly decreases, and the reflection rises strongly. The absorption behaviour already mentioned, viz. A rises to a maximum and drops towards higher electron densities, is particularly pronounced for $d = 2\,\lambda$.

It emerges from the foregoing remarks that the absorption calculated according to Eq. (8) is close to the values determined from the correct Eq. (11) as long as reflection is not too large. According to Fig. 7 this is the case when ω_p does not exceed the laser frequency ω at any point of the profile or, according to Sections II and III, when the laser power Φ_0 does not exceed the value $1.8 \times 10^{11}\,\mathrm{W^5cm^2}$. It can therefore be regarded as proved that already at relatively low intensities $\Phi_0 \geqq 2 \times 10^{11}\,\mathrm{W/cm^2}$ there is an overdense region $(\omega_p > \omega)$ in the plasma in the immediate vicinity of the cold phase. The limiting intensity is probably lower still because our calculations made no allowance for the reduction of the ionization energy, which at high densities can be quite large but is very difficult to state numerically (according to the Debye theory it should be about 8 eV); in addition, the Saha equation always gives too low values for the degree of ionization in the heating phase if the recombination time is not short enough (cf. Section V). As soon as we have $\omega_p > \omega$, of course, the wave equation has to be solved in order to obtain exact information on the electron densitites that actually occur.

At the point in the plasma where the WKB condition is no longer satisfied the original intensity Φ_0 in our intensity range has dropped to at least 1/4 owing to absorption. This immediately explains why only a small amount of reflection is observed in the experiment [16]; for even with total reflection in the overdense layer the remaining intensity would be reduced by at least 3/4 in the region of low electron

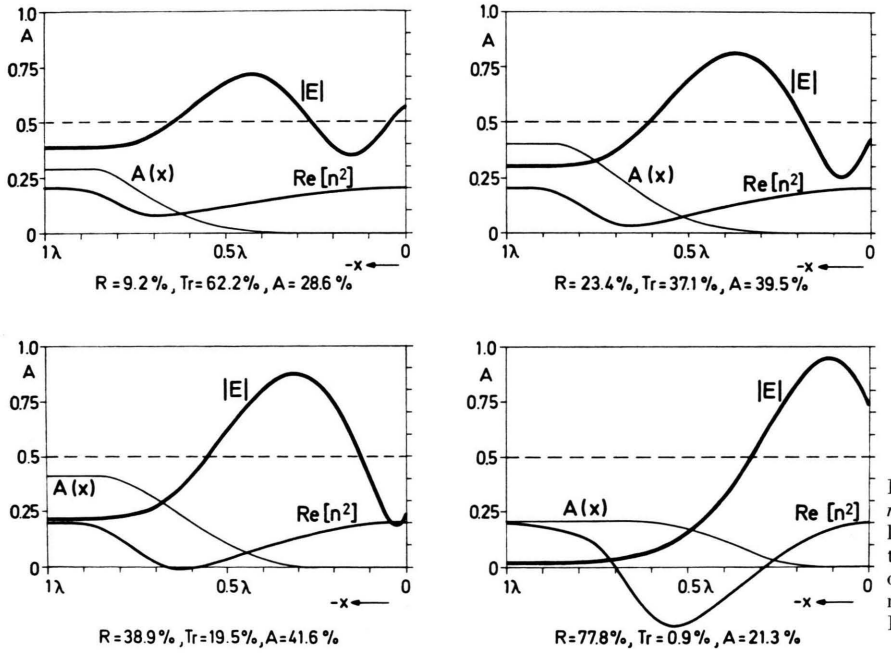

Fig. 6. Variation of the real part of n^2, variation of $|E|$ and normalized light absorption $A(x)$ for profiles of thickness $d = \lambda$ and various electron densities. R, Tr, A reflection, transmission and absorption coefficients. Irradiated from the right. Arbitrary units on right ordinate.

[16] R. SIGEL, Thesis Technische Hochschule München (1969) or IPP 3/96 [1969].

density on its way back, i.e. 1/16 of the original intensity at most would be observed as reflected light. It is not until sub-nanosecond laser pulses of extremely high intensity are applied that considerable reflection of up to 45% [17] occurs because in this case the expanded plasma in front of the transition region is absent.

V. Discussion

The basic equations in Section II are subject to two esesntial conditions; firstly, that the plasma production and heating processes can be described by hydrodynamic theory and, secondly, that a thermal model with $T_i = T_e = T$ (T_e, T_i electron and ion temperature) may be used. The momentum equation (2) is valid if the pressure in the numerical results changes only slightly over a mean free path l_i; i.e. $l_i \frac{1}{p} \frac{\partial p}{\partial x} \ll 1$, or if, according to [9], p. 258 and 438 and with the aid of Eq. (1),

$$4.3 \times 10^{-18} \frac{T^2}{\ln \Lambda} \frac{1}{n_i T} \frac{\partial (n_i T)}{\partial a} \ll 1 \quad [\text{cgs grad}].$$

This inequality is in fact very well satisfied in all calculations. – The critical point for the application of a thermal model with the electron temperature equal to the ion temperature is in the transition region from the cold phase to the thin, hot plasma. Figures 3 and 5 show that the temperature here rises almost linearly to 10^6 °K and enters the dense phase between 0.5 and 1 nsec with the velocity $\dot{d} = 6.5 \times 10^5$ cm/sec. Since this increase in the calculation covers four space steps $\Delta a = 2 \times 10^{-5}$ cm (see Appendix II), we get the characteristic reference time $\tau_0 = 4\, \Delta a / \dot{d} = 1.2 \times 10^{-10}$ sec. At the point $T = 10^6$ °K the normalized particle density is $N = n_H / n_0 = 0.1$. The following relaxation times ($\ln \Lambda = 5$) are now calculated according to [9] for the values:
Thermalization time for ions:

$$\tau_{ii} \approx \frac{1}{\nu_{ii}} = 6 \times 10^{-12} \text{ sec};$$

Thermalization time for electrons:

$$\tau_{ee} \approx \tau_{ii} \left(\frac{m_e}{m_i} \right)^{1/2} = 1.4 \times 10^{-13} \text{ sec};$$

Equipartition time for $T_i = T_e$:

$$\tau_{ei} \approx \tau_{ee} \frac{m_i}{4\, m_e} = 6.5 \times 10^{-11} \text{ sec}.$$

These times are appreciably shorter than τ_0, and so it seems certain that there is equilibrium in the transition region as well.

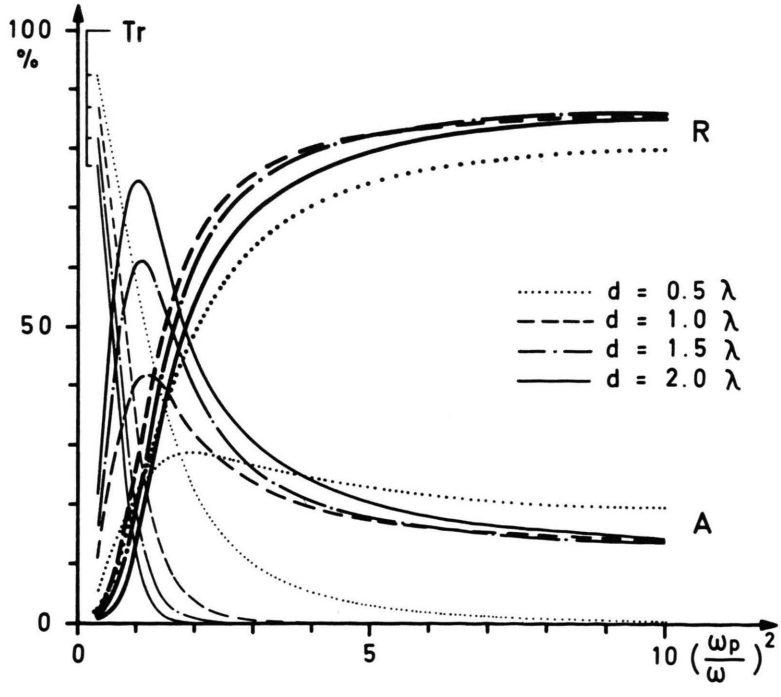

Fig. 7. Transmission Tr, reflection R, and absorption A as functions of the maximum normalized plasma frequency for layer thicknesses $d = 0.5$, 1, 1.5, and 2 λ.

[17] N. G. Basov, B. A. Boiko, O. N. Krokhin, O. G. Semenov, and G. V. Sklizkov, ZHTF **38**, 1973 [1968].

Saha equilibrium is obtained when the ionization and recombination rates are sufficiently high. Estimates according to [8], Vol. I, p. 389 et seq. yield ample ionization rates for applying the Saha equation. It is more difficult to obtain concrete information on the recombination times. Should these in fact be very long (which is certainly the case for very low degrees of ionization well below 0.7%), the Saha equation yields a lower limit for the electron density in the narrow, not completely ionized part of the transition region. This, however, is completely sufficient for our purposes since our aim in this connection has been to show that a strongly absorbing layer has to form in a plasma produced from solid hydrogen and that there are layers in the transition region where the plasma becomes overdense ($\omega_p > \omega$). The value for the initial degree of ionization used in Section III, $\eta = 7 \times 10^{-3}$ is arbitrary to a certain extent. Test calculations showed, that the special choice of the value for the initial ionization only has an effect in the first few nanoseconds, provided it is not too small (e. g. 10^{-10}) since ionisation-recombination equilibrium is not even approximately obtained in such a case.

The transition region is characterized by high densities and strong gradients. There is some uncertainty here as regards the equation of state and transport parameters. The absorption coefficient (6a), for example, may assume extremely high values. Numerical test calculations with widely varying coefficients for the dense region ($2 \cdot 10^{-2} \leqq \varrho/\varrho_0 \leqq 1$) – more than a factor 10^3 for the absorption coefficient – did show differences in the density, temperature, and velocity distributions in the immediate vicinity of the solid (up to a factor of 2), but such variations have almost no influence ($\leqq 6\%$) on the properties of the thin plasma ($\varrho/\varrho_0 \leqq 10^{-2}$), and the characteristic behaviour described in Section III persists in all regions. The curves in Fig. 5 for the quantity of plasma produced proved to be particularly insensitive (deviations below 2%).

In these calculations the collision frequency in the absorption coefficient is assumed to be caused by purely thermal motion. This is justified as long as the oscillation energy represents only a small fraction of the thermal energy of the plasma, as is the case here. In the coefficient of thermal conductivity allowance was made only for Coulomb interaction since only very close to the solid the plasma is not completely ionized and there thermal conduction is almost insignificant because of the lower temperature. Taking the electron-neutral collisions into account reduces thermal conduction in this region even more.

The true equation of state for hydrogen in the cold compressed phase is not known. The experimental investigations in [18] show very high compressibility for liquid hydrogen, and the assumption of Lennard-Jones interaction between the molecules does not yield correct results. On the other hand, we are not interested here primarily in the shock wave, but only insofar as it can modify the calculations for the hot plasma. It may be stated with certainty that the true compressibility of the solid hydrogen is between zero (incompressible solid) and that of an ideal gas, but closer to the latter. In order to obtain some idea of the influence of the equation of state of the cold phase on the heating of the plasma, the case of an incompressible solid was also calculated. The differences in temperature and density after 14 nsec in the plasma produced are shown in Fig. 8. The maximum error in the density is 18%, but it is under 10% over wide ranges. The largest relative error in the temperature is found to be 7.2%. It should be pointed out, however, that Fig. 8 misrepresents the values as too high, this being due to the fact that the incompressible case was calculated only for an infinitely extended solid (no reaction present), while the solid curves refer to a 50 μ foil accelerated to the left. The special form of the equation of state in the solid phase has very little influence on the quantity of plasma produced. After 20 nsec the difference in the quantity of plasma for compressible and incompressible hydrogen is less than 1%.

Even if the electron densities calculated with the Saha equation are too low in the transition region, they are still sufficient for forming a very strongly absorbing layer which prevents uniform heating of the foils and results in a strong shock wave. The conditions when small pellets are irradiated are similar, provided the laser intensity rises fast enough. "Burn-through" from one side of a foil has been convincingly demonstrated [16]. This, however, does not contradict the experimental findings that the plasma obtained by evaporating a drop espands almost isotropically after a relatively short time.

[18] M. VAN THIEL and B. J. ALDER, Mol. Phys. **10**, 427 [1966].

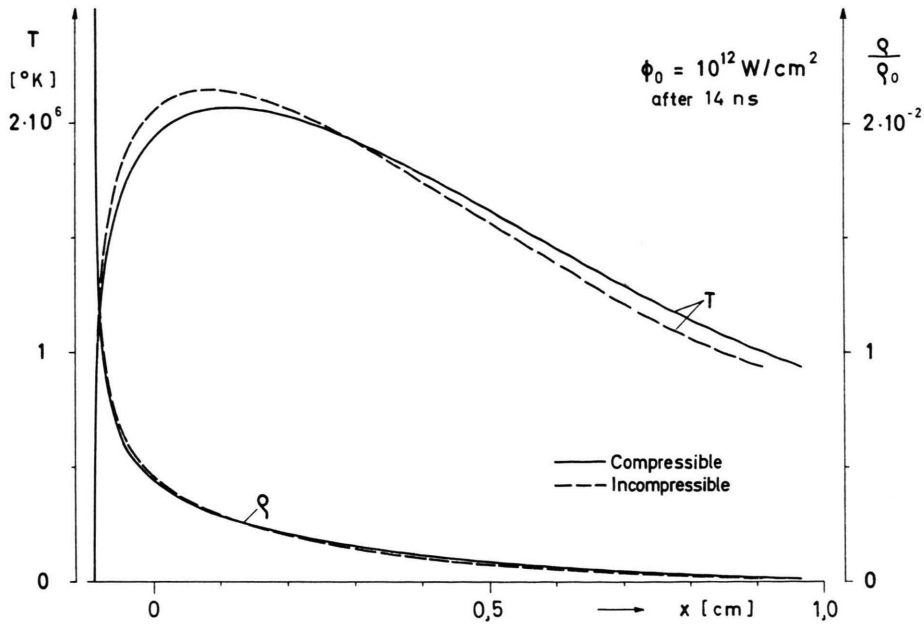

Fig. 8. Differences of temperature and density in the plasma for a compressible (ideal gas equation) and an incompressible solid.

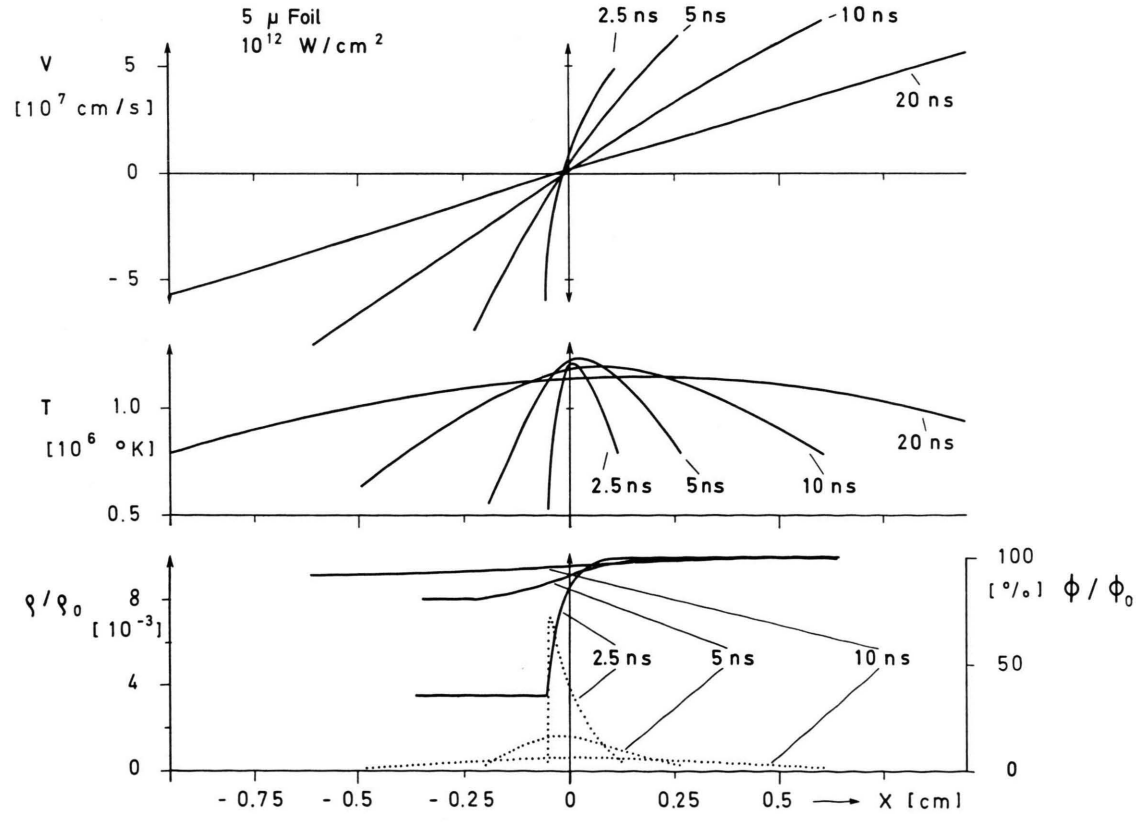

Fig. 9. Heating of a 5 μ thick foil and development of a symmetric plasm distribution. The solid curves below give the intensity, the dotted curve the density distribution. $\Phi_0 = 10^{12}$ W/cm^2. Irradiated from the right.

This can be seen by following up the heating of a thin foil beyond its burn-through time in our plane model, as in Fig. 9. One can readily trace the development to a symmetrical distribution of velocity, temperature and density.

All of the results in this paper refer to a one-dimensional plane model. With the laser intensities at present available such a case cannot be achieved experimentally. In experiments actually conducted the plasma is always more or less rotation symmetric since the high radiation densities required can only be obtained by focusing the laser light. The analogue calculations for such a geometry were felt, however, to be too cumbersome, especially since the heating process can readily be studied qualitatively in a one-dimensional model and the deviation estimated. In the experiments conducted hitherto the hot plasma can also expand to the sides, some of it already escaping from the radiation field of the laser after a short time. This reduces the temperatures attained theoretically in the one-dimensional case, which means that for a given incident energy the temperature has to be distributed over more particles with the result that a larger quantity of plasma is produced (cf. the comparison of theory and experiment in [16]).

Appendix I
Absorption Coefficient

In the Maxwell equations

$$c^2 \nabla \times \mathfrak{B} = \mathfrak{j}/\varepsilon_0 + \dot{\mathfrak{E}}\,,$$
$$\nabla \times \mathfrak{E} = -\dot{\mathfrak{B}}$$

the electric field strength is represented by that of a monochromatic light wave. Neglecting the polarization current one gets for the current density

$$j = n_e e \dot{y}$$

(y perpendicular to x). Furthermore, the equation of motion of free, not too fast electron is

$$\ddot{y} + \nu \dot{y} = (e/m) E \tag{1a}$$

where the Lorentz force is neglected and ν is the collision frequency. By substituting the solution of Eq. (1a) in the expression for j one obtains the following stationary wave equation for a plane electromagnetic wave $E = E(x,t)\, e^{-i\omega t}$ with amplitude varying slowly with time:

$$E'' + k^2 n^2(x,t)\, E = 0 \tag{2a}$$

and j itself is proportional to E: $j = \sigma \cdot E$, where the high frequency conductivity σ is related to the refractive index n by

$$(i\,\sigma/\varepsilon_0\,\omega) = n^2 - 1 \tag{3a}$$

($k = \omega/c$ is the wave vector in vacuum). The complex refractive index $n = n_R + i\, n_I$ is then expressed by means of the electron plasma frequency $\omega_p = (n_e\, e^2/\varepsilon_0\, m_e)^{1/2}$ as follows:

$$n^2 = (n_R + i\, n_I)^2 = 1 - \left(\frac{\omega_p}{\omega}\right)^2 \frac{1}{1+(\nu/\omega)^2} + i\,\frac{\nu}{\omega}\left(\frac{\omega_p}{\omega}\right)^2 \frac{1}{1+(\nu/\omega)^2}\,. \tag{4a}$$

If $\left| \frac{1}{2\,k^2 n^2}\left\{\frac{n''}{n} - \frac{3}{2}\left(\frac{n'}{n}\right)^2\right\}\right| \ll 1$, the solution of the wave equation is

$$E = \frac{E_0}{\sqrt{n}} \exp\left\{i\,k \int_x^\infty n\,\mathrm{d}x\right\} = \frac{E_0 \exp\{-k\int_x^\infty n_I\, x\}}{\sqrt{n}} \exp\left\{i\,k \int_x^\infty n_R\,\mathrm{d}x\right\}$$

(WKB approximation; see, for example [19], p. 181). As long as n_I is small relative to n_R, one obtains for the intensity using the relation for the group velocity $v_{gr} = c\, n_R$ (s. [19], p. 232)

$$\Phi(x,t) = \frac{\varepsilon_0\, v_{gr}}{2}\,\frac{E_0\, E_0^*}{n_R} \exp\left\{-2\,k\int_x^\infty n_I\,\mathrm{d}x\right\} = \frac{\varepsilon_0\, c}{2}\, E_0\, E_0^* \exp\left\{-2\,k\int_x^\infty n_I\,\mathrm{d}x\right\} = \Phi_0 \exp\left\{-\int_x^\infty \alpha\,\mathrm{d}x\right\} \tag{5a}$$

with the absorption coefficient $\alpha = 2\,k\,n_I$. Solving (4a) for n_I yields for α

$$\alpha = 2\,k \sqrt{\frac{1}{2}\left\{\sqrt{\left[1 - \left(\frac{\omega_p}{\omega}\right)^2 \frac{1}{1+(\nu/\omega)^2}\right]^2 + \left[\frac{\nu}{\omega}\left(\frac{\omega_p}{\omega}\right)^2 \frac{1}{1+(\nu/\omega)^2}\right]^2} - \left[1 - \left(\frac{\omega_p}{\omega}\right)^2 \frac{1}{1+(\nu/\omega)^2}\right]\right\}}\,. \tag{6a}$$

for $\nu \ll \omega$ and $\omega_p < \omega$ (6a) reduces to the most comonly used formula

$$\alpha = \frac{\omega_p^2\, \nu}{c^2\, \omega^2 [1 - (\omega_p/\omega)^2]^{1/2}}\,. \tag{6a'}$$

The expression (6a) is somewhat more general than the formula (6a'), and so (6a) is always used in

[19] V. L. Ginzburg, The Propagation of Electromagnetic Waves in Plasmas, Perg. Press Ltd., Oxford 1964.

this paper. For the temperatures expected it holds that $h\nu \ll kT$. The induced emission must therefore be taken into account. The way in which α is derived means, however, that it is already contained in (6a) (cf., for example [8], p. 124).

The collision frequency ν has two components $\nu = \nu_{ei} + \nu_{en}$ corresponding to the electron-ion and electron-neutral collisions; ν_{ei} is taken from SPITZER [11], p. 83.

$$\nu_{ei} = \frac{\pi^{3/2}\, e^4\, Z^2\, n_H\, \eta}{2\, m_e^{1/2} (2\,k\,T)^{3/2}\, \gamma_E} \ln \Lambda \qquad [\text{cgs grad}].$$

For ν_{en} we take

$$A (n_H/n_0)\,(1-\eta)$$

(n_0 particle density in solid hydrogen). According to [20] the mean value for A is $A = 4.5 \times 10^{14}\,\text{sec}^{-1}$, this being roughly in agreement with theoretically determined cross sections.

It should also be mentioned that Spitzer's formula for ν_{ei} in hydrogen is not very different from that used by Dawson. The difference in fact is

$$\frac{\nu_{ei}^{\text{Spritzer}}}{\nu_{ei}^{\text{Dawson}}} = \frac{16}{3\pi}\,\gamma_E = 0.988\,.$$

Appendix II
Numerical Integration of the Equations of Motion

For numerical integration of the equations of motion (1), (2), (3), and the velocity (4) the explicit difference scheme listed below proved suitable. The lattice points have the indices (l, m) l for time, m for space; the time step is Δt, the space step Δa. The term q denotes the artificial viscosity, for which the expressions in [21], p. 216 were used. The expression for the thermal current was rearranged as follows:

$$-\varkappa \frac{\varrho}{\varrho_0}\frac{\partial T}{\partial a} = -\varkappa' \frac{\varrho}{\varrho_0} T^{5/2} \frac{\partial T}{\partial a} = -\frac{2}{7}\frac{\varrho}{\varrho_0}\varkappa' \frac{\partial T^{7/2}}{\partial a}$$

Difference scheme

1) $$\varrho_0 \frac{v_m^{l+1/2} - v_m^{l-1/2}}{\Delta t} = \frac{1}{\Delta a}\left\{ p_{m+1/2}^l - p_{m-1/2}^l + \frac{4}{3\,\Delta a}\left[\varrho_{m-1/2}^l \mu_{m-1/2}^l \left(v_{m-1}^{l-1/2} - v_m^{l-1/2}\right) - \varrho_{m+1/2}^l \cdot \left(v_m^{l-1/2} - v_{m+1}^{l-1/2}\right)\right] \frac{1}{\varrho_0} \right\} - \frac{\Delta q}{\Delta a}$$

2) $$v_m^{l+1/2} = \frac{x_m^{l+1} - x_m^l}{\Delta t}\,,$$

3) $$\varrho_{m+1/2}^{l+1} = \frac{\varrho_0\, \Delta a}{x_m^{l+1} - x_{m+1}^{l+1}}\,,$$

4) $$\varrho_0 \frac{\varepsilon_{m+1/2}^{l+1} - \varepsilon_{m+1/2}^l}{\Delta t} = \frac{1}{\Delta a}\left\{ \Phi_m^l - \Phi_{m+1}^l + \left(v_{m+1}^{l-1/2} - v_m^{l-1/2}\right)\left[p_{m+1/2}^l + q_{m+1/2}^l - \frac{4}{3\,\varrho_0\,\Delta a}\,\varrho_{m+1/2}^l \mu_{m+1}^l \cdot \left(v_{m+1}^{l-1/2} - v_m^{l-1/2}\right)\right] + \frac{2}{7\,\varrho_0 \cdot 2\,\Delta a}\left[\varrho_{m-1/2}^l \varkappa'^l_{m-1/2} + \varrho_{m+1/2}^l \varkappa'^l_{m+1/2}\right)\left(T^{7/2\,l}_{m-1/2} - T^{7/2\,l}_{m+1/2}\right)\right] - \frac{2}{7\,\varrho_0\,\Delta a}\left[\left(\varrho_{m+1/2}^l \varkappa'^l_{m+1/2} + \varrho_{m+3/2}^l \varkappa'^l_{m+3/2}\right)\left(T^{7/2\,l}_{m+1/2} - T^{7/2\,l}_{m+3/2}\right)\right] \right\}.$$

The signs of the individual terms are due to the fact that the m-subscripts are counter to the a-direction. Solution of ε for the temperature T was done by the nested interval method.

Step sizes: For given $\Delta a = 2 \times 10^{-5}$ cm and laser intensities below $4 \times 10^{12}\,\text{W/cm}^2$ a time step $\Delta t = 10^{-12}$ sec was chosen; for higher Φ_0 the Δt was half as large. This is because the time step has to be made at least so small that the inequality $|\Delta v_m|\,\Delta t < |\Delta x_m|$ is satisfied at all lattice points. A further condition is imposed, on the ratio $\Delta t/\Delta a$ and on Δa itself. Owing to the finite space and time step sizes it is not possible to determine the velocity of the plasma front, i. e. the velocity of the plasma-vacuum interface; the calculation has to be truncated towards the vacuum at a finite thick-

[20] W. P. ALLIS and S. C. BROWN, Phys. Rev. **87**, 419 [1952].

[21] R. D. RICHTMYER, Difference Methods for Initial-Value Problems, Intersc. Publ. Inc., New York 1957.

ness. This may result in errors propagating into the interior of the plasma. The difference scheme was therefore tried out on an adiabatic rarefaction wave for which the solution can also be given in closed form. Excellent agreement was obtained using the above step sizes. In calculating the thermal conduction it was ensured that no heat can flow into the vacuum by introducing an appropriate boundary condition. After every 500 time steps the conservation of energy and momentum was checked by integrating the appropriate quantities over space. The relative errors are below 0.1%.

This work was undertaken as part of the joint research programme between the Institut für Plasmaphysik and Euratom.

Acknowledgement

The author wishes to thank Prof. Dr. R. WIENECKE for his support and encouragement. He is also indebted to Dr. S. WITKOWSKI for numerous discussions.